PHYSICAL REVIEW C 77, 034301 (2008)

# Toward $^{100}$Sn: Studies of excitation functions for the reaction between $^{58}$Ni and $^{54}$Fe ions

A. Korgul,[1,2,3,4] K. P. Rykaczewski,[5] C. J. Gross,[5] R. K. Grzywacz,[3] S. N. Liddick,[3,6] C. Mazzocchi,[3,7] J. C. Batchelder,[8] C. R. Bingham,[3] I. G. Darby,[3] C. Goodin,[4] J. H. Hamilton,[4] J. K. Hwang,[4] S. V. Ilyushkin,[9] W. Królas,[10] and J. A. Winger[2,8,11]

[1]*Institute of Experimental Physics, Warsaw University, PL 00-681 Warszawa, Poland*
[2]*Joint Institute for Heavy-Ion Research, Oak Ridge, Tennessee 37831, USA*
[3]*Department of Physics and Astronomy, University of Tennessee, Knoxville, Tennessee 37996, USA*
[4]*Department of Physics and Astronomy, Vanderbilt University, Nashville, Tennessee 37235, USA*
[5]*Physics Division, Oak Ridge National Laboratory, Oak Ridge, Tennessee 37831, USA*
[6]*UNIRIB, Oak Ridge Associated Universities, Oak Ridge, Tennessee 37831, USA*
[7]*IFGA, University of Milan and INFN, I-20133 Milano, Italy*
[8]*UNIRIB, Oak Ridge Associated, Oak Ridge, Tennessee 37831, USA*
[9]*Department of Physics and Astronomy, Mississippi State, Mississippi 39762, USA*
[10]*Institute of Nuclear Physics, Polish Academy of Sciences, PL 31-342 Kraków, Poland*
[11]*Department of Physics and Astronomy, Mississippi State University, Mississippi 39762, USA*
(Received 6 November 2007; published 7 March 2008)

Production of nuclei above $^{100}$Sn in fusion-evaporation reactions between $^{58}$Ni and $^{54}$Fe ions was studied at Oak Ridge National Laboratory by means of the recoil mass spectrometer and charged particle detection. The beam energy was varied to optimize the yields for the two-, three- and four-particle evaporation channels. Experimental results verified the predictions of the statistical model code HIVAP. The optimum energy for the $^{54}$Fe($^{58}$Ni,4$n$)$^{108}$Xe reaction channel that allows one to study the $^{108}$Xe-$^{104}$Te-$^{100}$Sn $\alpha$ decay chain is deduced as 240 MeV.

DOI: 10.1103/PhysRevC.77.034301 PACS number(s): 29.30.Ep, 23.60.+e, 25.70.Gh, 27.60.+j

## I. INTRODUCTION

The region of nuclei around the doubly magic $^{100}$Sn is unique in the nuclear landscape. It allows us to study the structure of nuclei near closed shells ($N = Z = 50$) located in the vicinity of the proton drip line. The decay properties of proton-rich nuclei near $^{100}$Sn also have an astrophysical importance related to the final phase of nucleosynthesis within the rapid proton capture ($rp$) process. The fast charge particle decays of antimony and tellurium isotopes lead to a Sn-Sb-Te cycle terminating the $rp$-process and preventing the creation of elements above $Z = 52$ via subsequent proton capture [1,2]. In this work, we investigate the yields of nuclei above $^{100}$Sn to establish the optimum way to observe the $^{108}$Xe-$^{104}$Te-$^{100}$Sn $\alpha$ decay chain.

Doubly magic $^{100}$Sn and its nearest neighbors are very difficult to reach experimentally. Only 11 and 24 ions of $^{100}$Sn were first identified among the fragmentation products of 1 GeV/nucleon $^{124}$Xe [3] and 63 MeV/nucleon $^{112}$Sn [4,5] beams, respectively. The estimated production cross sections were as low as 12 and 120 pb for these $^{124}$Xe [3] and $^{112}$Sn [4,5] beams, respectively. Further fragmentation-based attempts did not result in increased statistics of $^{100}$Sn events [6,7]. One event of $^{100}$Sn identified among the 1 GeV/nucleon $^{112}$Sn fragmentation products [7] corresponds to a production cross section of ~2 pb.

Nearly symmetric fusion-evaporation reactions between heavy ions offer larger cross sections for the production of nuclei in the $^{100}$Sn region. The mass measurement [8] of $^{100}$Sn was based on about ten ions produced in the reaction $^{50}$Cr+$^{58}$Ni at 255 MeV. The reported cross section value was as high as 40 nb [8]. A lower value of ≈3 nb was estimated for the production of $^{100}$Sn in the collisions of $^{58}$Ni and $^{50}$Cr nuclei from decay studies of proton-rich tin isotopes at the GSI on-line mass separator [9]. It is based on the experimental yields obtained with ≈3 mg/cm$^2$ thick targets for the $A =$ 101–105 tin isotopes including the value of ~60 nb derived for $^{101}$Sn (see also Ref. [10]). The cross section decrease is nearly logarithmic when approaching $^{100}$Sn [9]. In both studies [8,9], the observed yields of proton-rich tin isotopes were converted into cross section values using the estimated efficiencies of processes involved in the selection of specific isotopes. In particular, the transmission efficiency of the ion optics system is not measured directly, but estimated based on the data from somewhat similar reactions and/or calculated using ion optics simulations. For the on-line mass separator studies, corrections include averaging over target thickness, half-life dependent ion source release efficiency, beam line transmission, and absolute branching ratios calculated for the detected radiation [9,10]. Therefore, differences between quoted "apparent" experimental cross sections might eventually occur.

This work makes use of charge particle decay to establish the optimum conditions for studying exotic proton-rich nuclei near $^{100}$Sn by means of the recoil mass spectrometer (RMS) technique [11]. The analyzed yields for the 2$n$, 3$n$, and $p$3$n$ evaporation channels are used to deduce the optimum beam energy of $^{58}$Ni projectiles on $^{54}$Fe targets for producing $^{108}$Xe after 4$n$ evaporation. The $\alpha$ decay of $^{108}$Xe will eventually lead to $^{100}$Sn via a super-allowed $\alpha$ transition from $^{104}$Te [12–15]. The results of the studies presented here have already helped to identify the new $\alpha$ decay chain $^{109}$Xe-$^{105}$Te-$^{101}$Sn [13] and to find a very weak $\alpha$ decay branch in the decay of the ground-state proton emitter $^{109}$I [2].

 ©2008 The American Physical Society

## II. EXPERIMENTS

The experiments were performed at the recoil mass spectrometer [11] at the Holifield Radioactive Ion Beam Facility (HRIBF) at Oak Ridge National Laboratory. Beams of $^{58}$Ni on $^{54}$Fe targets leading to the compound nucleus $^{112}$Xe were used to produce charge particle emitters above tin isotopes. The nuclei recoiling from the target were separated according to their mass-to-charge ($A/Q$) ratio. Ions in two charge states were transmitted to the RMS final focus (converging ion optics [11]). After passing through the position sensitive microchannel plate detector (MCP) [16], the recoils were implanted into the double-sided silicon strip detector (DSSD). The implantation and decay signals were recorded using digital signal processing in XIA DGF 4C modules [17–20]. For longer lived activities, the standard acquisition mode was used, and the signal time and amplitude were analyzed onboard. A different technique for the signal acquisition mode was developed to study the decays involving the pileup of two $\alpha$ signals such as in the $^{110}$Xe-$^{106}$Te-$^{102}$Sn and $^{109}$Xe-$^{105}$Xe-$^{101}$Sn decay chains [13,19,20].

The energies of $^{58}$Ni projectiles were varied between 195 and 265 MeV, and the $^{54}$Fe target thickness was 470 $\mu$g/cm$^2$. The $^{58}$Ni beam energy loss over the thickness of this $^{54}$Fe target is about 10–11 MeV. The charge states of recoils ranged from $25^+$ to $30^+$. A 20 $\mu$g/cm$^2$ carbon charge reset foil was placed about 10 cm after the target [11]. For each beam energy, different settings of the RMS ion optics were tested. The energy and charge states of the recoils were varied to achieve the maximum counting rate of the most exotic known isobar of a given mass $A$, i.e., $^{108}$I ($p3n$), $^{109}$I ($p2n$), and $^{110}$Xe ($2n$). For mass $A = 109$, the observed yields for the new isotope $^{109}$Xe produced in the $3n$ evaporation channel [13] are included in this presentation.

## III. CALCULATIONS

To estimate the appropriate beam energy, calculations were performed using a 1994 version of the GSI statistical model code HIVAP [21,22]. This relatively simple-to-use code is widely used in its default version to estimate beam energies and cross sections for experiments on proton-rich nuclei. The default mass table used in these calculations consisted of 1993 experimental masses [23] and Möller *et al.* extrapolations [24], see Table I. The particle separation energies and the shell and pairing corrections were obtained using this mass table (recommended option). The scaling parameter $r_0$ for level densities was set to 1.153 (recommended) instead of 1.16, which was used originally by Töke and Świątecki [25]. Liquid drop fission barriers [26] were used. However, according to the calculations, the fission probability is small for these light nuclei.

## IV. RESULTS

Examples of results for the production of $A = 110$ isobars in the $2n$, $3n$, and $4n$ reaction channels are displayed in Fig. 1. The beam energies E$_M$ are given at the middle of the target (calculated from the initial beam energy $E_B$ reduced by 5 MeV), while the calculated cross sections are averaged over the 10 MeV range. One notices a nearly flat profile for the cross section over a wide beam energy range for $^{110}$Xe produced in the $2n$ evaporation channel in the $^{58}$Ni+$^{54}$Fe reaction. It suggests a beam energy $E_B$ around 235–240 MeV as an optimum choice for production of $^{110}$Xe and $^{109}$Xe, and the energy of ~270 MeV for production of $^{108}$Xe. However, the experimental yields, see Fig. 2, clearly indicate narrower distributions, with the beam energy $E_B$ that maximizes the production of $^{110}$Xe being lower by as much as 20–30 MeV. Nearly the same beam energy corresponds to the optimum production of the less exotic $^{110}$I in the ($pn$) channel. The experimental yields were corrected for the total efficiency of our setup. The $\alpha$ and proton detection efficiencies of the DSSD were simulated with GEANT [27]. For example, for deeply implanted 65 MeV recoils of $^{110}$Xe and 70 MeV recoils of $^{109}$I, detection efficiencies for the 3.72 MeV $\alpha$ particles and 0.81 MeV protons were calculated to be (85±2)% and (97±3)%, respectively. The errors result from the energy spread of the recoils. The RMS transmission was measured earlier for recoils produced using a 212 MeV $^{58}$Ni beam and a 400 $\mu$g/cm$^2$ $^{28}$Si target with a 900 $\mu$g/cm$^2$ Ta front layer, by correlating the $\gamma$-$\gamma$ coincidences recorded at the target with the number of RMS-transmitted ions. Efficiencies of 5.2% and 4.1% were obtained for the $3p$ ($^{83}$Y) and $\alpha 2p$ ($^{80}$Sr) evaporations channels [11], which are similar enough to the reactions in the presented work. Therefore, a constant efficiency of (5±1)% was adopted for the transmission of all recoils in two charge states to the implantation detectors in the RMS final focus. The 20% uncertainty should adequately reflect differences in reaction kinematics and target variations between the past and present work. The observed yields given in ions/s at 1 pnA beam intensity given in Fig. 2 were converted into cross sections (left vertical axis) averaged over the 470 $\mu$g/cm$^2$ target thickness. The relative 20% error resulting

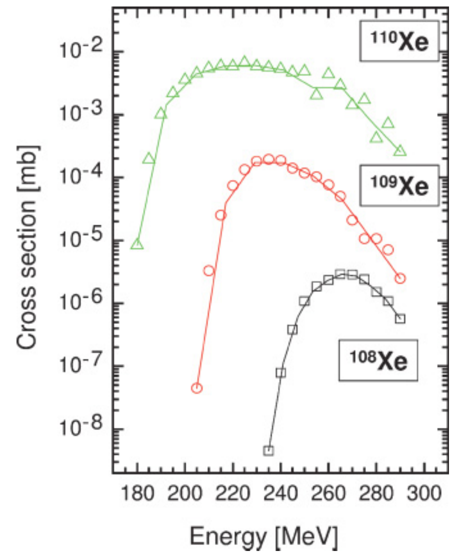


FIG. 1. (Color online) Cross section distribution obtained using a 1994 version of the HIVAP code for $^{110}$Xe, $^{109}$Xe, and $^{108}$Xe produced in the $^{58}$Ni+$^{54}$Fe reaction.

TABLE I. Neutron ($S_n$), proton ($S_p$), and $\alpha(S_\alpha)$ separation energies (in MeV) used as the input values in two sets of the HIVAP code calculations described in the text. The updated $S_n$, $S_p$, $S_\alpha$ values are based on Refs. [9,13,28–31]. The mass excess values (ME) correspond to the updated separation energies.

| Nuclide | Default values | | | Updated values | | | |
|---|---|---|---|---|---|---|---|
| | $S_n$ | $S_p$ | $S_\alpha$ | $S_n$ | $S_p$ | $S_\alpha$ | ME |
| $^{110}$Xe | 13.88 | 0.61 | −4.44 | 14.37 | 1.58 | −3.89 | −51.90 |
| $^{109}$Xe | 12.07 | 0.19 | −4.69 | 12.07 | 0.24 | −4.22 | −45.60 |
| $^{105}$Te | 11.80 | 0.38 | −4.92 | 11.80 | 0.35 | −4.90 | −52.24 |
| $^{103}$Sn | 10.27 | 4.11 | −0.48 | 10.05 | 3.54 | −0.47 | −66.96 |
| $^{102}$Sn | 13.26 | 3.63 | −0.29 | 13.49 | 3.66 | −0.05 | −64.98 |

from the transmission efficiency estimate of (5±1)% is not included in the error bars displayed in the Figs. 2–4. This means that all experimental cross section points can be moved up or down simultaneously, within ±20% of their values, with respect to the calculated values. However, it does not change the shape of the experimental excitation function or the derived optimum beam energy.

We have repeated the HIVAP calculations using updated mass values [28] and recent experimental results [9,13,29–31]. The relevant changes to the input mass values are listed in Table I. The recalculated distributions drop more quickly for higher beam energies and better fit the experimental data for the $^{110}$Xe and $^{110}$I, as seen in Fig. 2. This indicates that our results depend strongly on the mass values used.

The measurements performed for $^{110}$Xe and $^{110}$I recoils guided our study of $A = 109$ activities. The experimental yield curves obtained for $^{109}$I and $^{109}$Te, see Fig. 3, suggested a

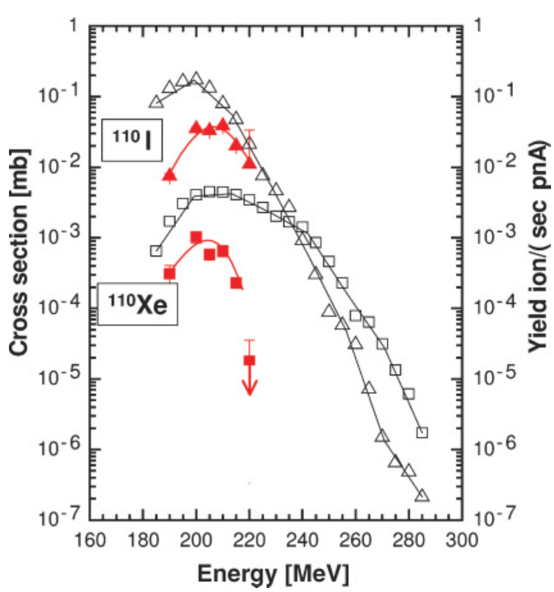


FIG. 2. (Color online) Experimental yields (right axis) for *pn* and 2*n* fusion-evaporation channels in the $^{58}$Ni+$^{54}$Fe reaction (solid symbols) vs projectile energy in the middle of the target. These yields were converted into cross section values (left axis). The predictions of the statistical model code HIVAP (open symbols) obtained with updated input mass values (see Table I) are compared with our experimental data. The error bars of the experimental points, some of them smaller than the symbols used, include the statistical uncertainties of the observed number of counts and the particle detection efficiency, while the 20% relative error of the constant (5±1%) RMS transmission is not included; see text for more details.

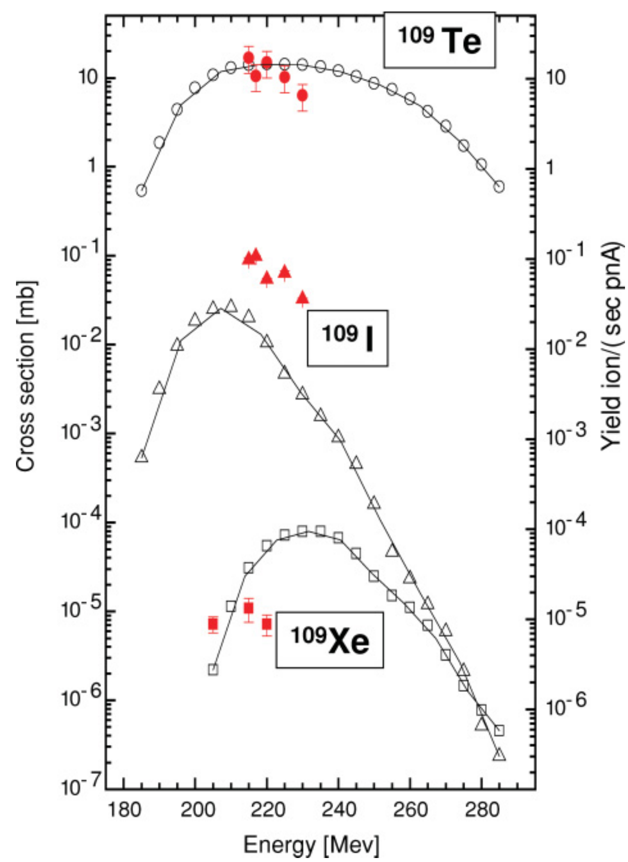


FIG. 3. (Color online) Comparison of the experimental data (solid symbols) for the production of $^{109}$Te, $^{109}$I, and $^{109}$Xe in the fusion reaction $^{58}$Ni+$^{54}$Fe, and respective cross section values predicted with the statistical model code HIVAP (open symbols) using the updated particle separation energy values. The error bars of the experimental points, some of them smaller than the symbols used, include the statistical uncertainties of the observed number of counts and the particle detection efficiency, while the 20% relative error of the constant (5±1)% RMS transmission is not included; see text for more details.

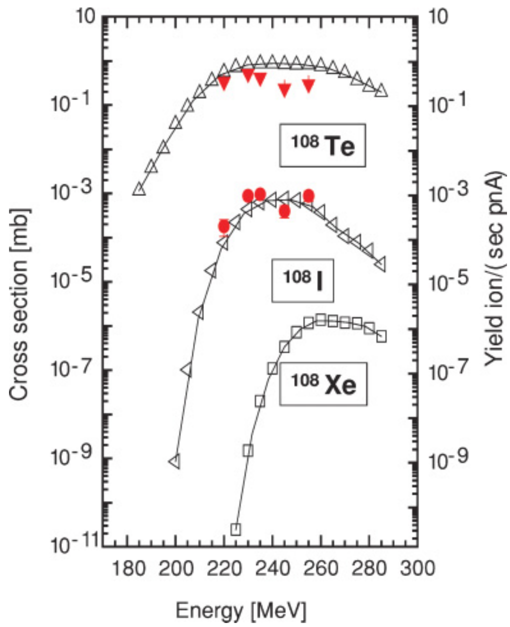


FIG. 4. (Color online) Experimental yields (solid symbols) for four-particle evaporation products from the fusion reaction $^{58}Ni+^{54}Fe$ and HIVAP predictions (open symbols) obtained with updated particle separation energy values. The error bars of the experimental points, some of them smaller than the symbols used, include the statistical uncertainties of the observed number of counts and the particle detection efficiency, while the 20% relative error of the constant (5±1)% RMS transmission is not included; see text for more details.

beam energy $E_B$ of 220–225 MeV, close to the maximum for $^{109}$I and $^{109}$Te. The search for $^{109}$Xe was performed with beam energy $E_B$ of 222 MeV and was indeed successful [13]. The HIVAP calculations with modified masses for $A = 109$ isobars are shown for comparison in Fig. 3. The experimental optimum beam energies are nearly reproduced. Interestingly, the optimum beam energy (optimum excitation energy of the compound nucleus $^{112}$Xe) is practically the same, $E_B$ of 220–225 MeV for production of $^{109}$I and $^{109}$Xe, similar to the excitation functions for $^{110}$I and $^{110}$Te peaking at the same beam energy $E_B$ of about 200 MeV.

Similar studies were performed for the $A = 108$ isobars, see Fig. 4. The agreement between the measured yield curves converted into cross section and the calculated cross section values for $^{108}$Te and $^{108}$I is even better. Calculations still indicate a beam energy $E_B$ of about 265 MeV as the best choice for the production of $^{108}$Xe. However, based on the results of the mass $A = 110$ and $A = 109$ isobars, we estimate that a beam energy around 240 MeV will maximize the production of the $A = 108$ isobar $^{108}$Xe in the $^{58}Ni+^{54}Fe$ reaction. The cross section for the 4$n$ evaporation channel can be expected at the (sub)nanobarn level, see Fig. 4. At $\sigma = 1$ nb, the implantation of about 20 $^{108}$Xe ions can be achieved in 100 hr with 50 pnA beam intensity and a 300 $\mu g/cm^2$ $^{54}$Fe target. The targets rotating with the speed corresponding to a linear velocity for the irradiated spot of about 0.3 m/s can withstand this high beam intensity, see, e.g., Ref. [32]. The predicted half-lives of $^{108}$Xe and $^{104}$Te are of the order of 50 $\mu$s and 10 ns, respectively [14,15]. Using digital pulse processing and recording decay signal waveforms, one should be able to identify the pileup of two $\alpha$ signals at the sum energy around 10 MeV [15].

## V. SUMMARY

In summary, the previous attempts to directly produce $^{100}$Sn nuclei in fragmentation or in fusion-evaporation reactions were briefly reviewed. An alternative method to reach $^{100}$Sn via the $\alpha$ decay chain $^{108}$Xe-$^{104}$Te-$^{100}$Sn at the recoil mass separator was considered. The yields of the neighboring nuclei, $^{110}$Xe, $^{110}$I, $^{109}$Xe, $^{109}$I, $^{109}$Te, $^{108}$I, and $^{108}$Te were measured using the RMS technique. The experimental yields were converted into cross section values and compared to the predictions of the statistical model code HIVAP. Better agreement with experimental data was achieved after updating the mass table used in the calculations. The experimental results indicate that it is possible to produce the most proton-rich isobar through the $xn$ evaporation channel by choosing the optimum beam energy maximizing the yields for less exotic isobars. A $^{58}$Ni beam energy of ∼240 MeV corresponding to the $^{112}$Xe excitation energy of 58 MeV is proposed for production of $^{100}$Sn populated via the super-allowed $\alpha$ decay chain from the 4$n$ evaporation product $^{108}$Xe. Despite the short half-lives predicted for the $^{108}$Xe and $^{104}$Te $\alpha$ emitters, the detection of the sum $\alpha$ signal identifying the $^{108}$Xe-$^{104}$Te-$^{100}$Sn decay chain is possible during an ∼5 day experiment with a 50 pnA beam at the HRIBF recoil mass spectrometer.

## ACKNOWLEDGMENTS

This work was supported in part by the US DOE under Grant Nos. DE-AC05-060R23100, DE-FG02-96ER40983, DE-AC05-00OR22725, DE-FG02-96ER41006, and DE-FG05-88ER40407, the UNIRIB Consortium, the U.K. EPSRC, and the Foundation for Polish Science.

[1] H. Schatz *et al.*, Phys. Rev. Lett. **86**, 3471 (2001).
[2] C. Mazzocchi *et al.*, Phys. Rev. Lett. **98**, 212501 (2007).
[3] R. Schneider *et al.*, Z. Phys. A **384**, 241 (1994).
[4] M. Lewitowicz *et al.*, Phys. Lett. **B332**, 20 (1994).
[5] K. Rykaczewski *et al.*, Phys. Rev. C **52**, R2310 (1995).
[6] R. Grzywacz *et al.*, Phys. Rev. C **55**, 1126 (1997).
[7] A. Stolz *et al.*, Phys. Rev. C **65**, 064603 (2002).
[8] M. Chartier *et al.*, Phys. Rev. Lett. **77**, 2400 (1996).
[9] M. Karny *et al.*, Eur. Phys. J. A **25**, s01, 135 (2005).
[10] O. Kavatsyuk *et al.*, Eur. Phys. J. A **31**, 319 (2007).
[11] C. J. Gross *et al.*, Nucl. Instrum. Methods Phys. Res. A **450**, 12 (2000).
[12] R. D. Macfarlane and A. Siivola, Phys. Rev. Lett. **14**, 114 (1965).
[13] S. N. Liddick *et al.*, Phys. Rev. Lett. **97**, 082501 (2006).
[14] C. Xu and Z. Ren, Phys. Rev. C **74**, 037302 (2006).
[15] P. Mohr, Eur. Phys. J. A **31**, 23 (2007).
[16] D. Shapira *et al.*, Nucl. Instrum. Methods Phys. Res. A **454**, 409 (2000).

[17] W. K. Warburton *et al.*, Nucl. Instrum. Methods Phys. Res. A **422**, 41 (1999).
[18] R. K. Grzywacz, Nucl. Instrum. Methods Phys. Res. B **204**, 649 (2003).
[19] R. K. Grzywacz *et al.*, Nucl. Instrum. Methods Phys. Res. B **261**, 1103 (2007).
[20] S. N. Liddick *et al.*, Eur. Phys. J. Special Topics **150**, 131 (2007).
[21] W. Reisdorf *et al.*, Z. Phys. A **300**, 227 (1981).
[22] W. Reisdorf and M. Schädel, Z. Phys. A **343**, 47 (1992).
[23] G. Audi and A. H. Wapstra, Nucl. Phys. **A565**, 1 (1993).
[24] P. Möller *et al.*, At. Data Nucl. Data Tables **59**, 185 (1995).
[25] J. Töke and W. J. Swiatecki, Nucl. Phys. **A372**, 141 (1981).
[26] S. Cohen, F. Plasil, and W. J. Swiatecki, Ann. Phys. (NY) **82**, 557 (1974).
[27] S. Agostinelli *et al.*, Nucl. Instrum. Methods Phys. Res. A **506**, 250 (2003).
[28] G. Audi *et al.*, Nucl. Phys. **A729**, 337 (2003).
[29] Z. Janas *et al.*, Eur. Phys. J. A **23**, 135 (2005).
[30] M. Karny *et al.*, Eur. Phys. J. A **27**, 129 (2006).
[31] O. Kavatsyuk *et al.*, Eur. Phys. J. A **25**, 211 (2005).
[32] K. P. Rykaczewski, C. J. Gross, and R. K. Grzywacz, AIP Conf. Proc. **961**, 12 (2007).